



Melting behavior of sulfur-bearing silicate–phosphate glass batches

Justyna Sułowska¹ · Magdalena Szumera¹ · Dominika Madej¹ · Bartosz Handke¹ · Konrad Świerczek²

Received: 1 April 2022 / Accepted: 27 November 2022 / Published online: 19 December 2022
© The Author(s) 2022

Abstract

The main purpose of the research was to explain the differences between nominal and actual chemical compositions of silicate-phosphate glasses in the $\text{SiO}_2\text{-P}_2\text{O}_5\text{-K}_2\text{O-MgO-SO}_3$ system. The actual compositions of the materials were determined with X-ray fluorescence (XRF) analyses. Changes in the chemical composition were explained by examining the melting processes for selected glass batches with differential scanning calorimetry-thermogravimetry-related gas analysis by mass spectrometry (DSC-TG-EGA (MS)) and high-temperature X-ray diffraction (HT-XRD). It was found that changes in the chemical composition of the sulfur-bearing glasses were associated with the release of gaseous products. The main gases released during thermal decomposition of the selected glass batch were water vapor, carbon dioxide, carbon monoxide, and ammonia. Since these glasses have potential for use as glassy fertilizers, there is no doubt that the present study is important from an environmental point of view.

Keywords Silicate-phosphate glasses · Glass batch · Sulfur · DSC-TG-EGA (MS) · HT-XRD · Gas emission

Introduction

In 1969, Secretary-General of the United Nations U Thant drew attention to the crisis involving human attitudes toward the environment in his famous report "Man and His Environment" [1]. Since then and especially now, the clear emphasis is on reducing gas emissions into the atmosphere [2].

One of the sources of air pollution may be melting activities. This involves emission from a.o., since they often emit sulfur oxides, nitrogen oxides, carbon dioxide, and monoxide, hydrogen sulfide.

The sulfur oxides (SO_x) is related to the presence of sulfur in the fuel used for combustion, as well as to decomposition of sulfur compounds in the batch materials, particularly from the fining process with sulfates. Carbon dioxide (CO_2) is one of the major products of combustion. It is also emitted after decomposition of carbonates in batch materials (e.g., soda ash, limestone, and potash). Carbon monoxide (CO)

is the product of incomplete combustion. Hydrogen sulfide (H_2S) is formed from the fuel sulfur in hot blast cupolas due to the reducing conditions found in parts of the furnace. Nitrogen oxides are emitted from oxidation of the nitrogen in fuels and decomposition of nitrogen compounds in batch materials. Obviously, thermal NO_x can form at high melting temperatures, and NO_x can form promptly. Emission of these compounds should be limited, since they cannot be completely eliminated in glass melting processes [3]. According to [4], at least 90 mass% of the world's glass production uses sulfate raw materials to improve melting kinetics and fining. Batch reactions, especially in the presence of coke or organic components, influence the decomposition of sulfates or result in partial conversion to sulfides during batch melting [4, 5].

Sulfate exhibits several functionalities in the glass melting process in addition to fining, in which sulfate raw materials are intentionally added to glass-forming batches to enhance the removal of gas bubbles from freshly molten glass in glass furnaces; sulfates also act as oxidizing agents due to the release of oxygen upon heating the batch [5, 6] and coloring the glass. Sodium sulfate in combination with ferric iron (Fe^{3+}) results in formation of the chromophore required for amber glass [4].

Sodium and potassium carbonate are important components of high-temperature materials [7]. Therefore,

✉ Justyna Sułowska
sulowska@agh.edu.pl

¹ Faculty of Materials Science and Ceramics, AGH University of Science and Technology, Al. Mickiewicza 30, 30-059 Kraków, Poland

² Faculty of Energy and Fuels, AGH University of Science and Technology, Al. Mickiewicza 30, 30-059 Kraków, Poland

information on the gas phase is important for modeling long-term processes, for which the stabilities of the carbonates should be taken into account.

Heide [8] pointed out that the decomposition and volatilization reactions in glass batches are important factors for glass manufacturing, and they optimize the melting conditions and material properties, minimize the environmental impacts and effect complete utilization of raw materials. Therefore, it is worth studying the glass batch melting process.

Heating of glass batches involves numerous chemical reactions between solid phases, between the solid and liquid phase or between solid/liquid phases and gaseous phases [5, 9].

The methods most commonly used for this purpose are thermal analysis methods, including differential scanning calorimetry (DSC), differential thermal analysis (DTA), thermogravimetric analysis (TG), evolved gas analysis (EGA) coupled with gas chromatography and mass spectrometry [10, 11], high temperature in situ X-ray diffraction (HT-XRD) [11], and conventional XRD analysis [10].

Batch reactions of soda-lime-silica glasses heated up to 1300 °C have been investigated [11] with in situ X-ray diffraction. Cheng et al. [10] examined the influence of granulation on the behaviors of soda-lime-silica glass batches at temperatures of 775–900 °C with TG and conventional XRD analyses. Samples of the glass batches studied by Cheng et al. [10] were obtained by placing them in an electric furnace at temperatures of 775, 800, 825, 850 °C and then held at the specified temperature for different times (0–60 min). Deng et al. [12] studied the melting behavior of a representative commercial green container glass batch with and without addition of 15 mass% briquettes produced from fine waste cullet particles to reduce waste and glass melting energy. Deng et al. [12] prepared samples for research via a procedure similar to that of Cheng et al. [10], but the crucibles with glass batches were heated to 1450 °C and then subjected to conventional XRD analysis, as well as differential thermal analysis coupled with mass spectrometry (DTA-TGA-MS). Deng et al. [12] showed that adding briquettes to container glass batches had a positive effect by increasing the melting rate and lowering the batch reaction and decomposition temperatures.

Beerkens [5] investigated chemical reactions during glass batch heating for production of typical soda-lime-silica glasses, such as float and container glass compositions, but concentrated on the behavior of sulfur components during heating of glass batches in reduced melts containing coke or organic materials.

Gas release during melting and fining of sulfur-containing glass batches for soda-lime-silica glass production has been investigated [4] with evolved gas analyses. The glass batches presented in the work [4] also included organic components

or coke, which, as has already been mentioned, affected the decomposition of sulfates or resulted in the conversion to sulfides during batch melting. After batch melting, the remaining sulfur species further reacted with freshly molten glass still containing sand particles and gaseous inclusions. The authors conducted an EGA study on different batches containing organic components or coke under dry, wet, nitrogen, and simulated furnace atmospheres to investigate gas release (CO, CO₂, SO₂, O₂) and sulfur reactions during batch heating and glass melt fining. Obviously, research conducted in [4] showed that the gases mentioned above were emitted. This information is essential for predicting foaming and fining behavior and the final glass redox state (color of final glass) for batch compositions of industrially applied raw materials and for finding methods to reduce SO_x emissions.

Vernerová et al. [9] also identified and evaluated the crucial chemical reactions occurring during melting under different oxidizing–reducing conditions by evolving gas analysis (EGA) coupled with gas chromatography and mass spectrometry at temperatures up to 1500 °C. The main reactions of the initial sulfates were confirmed and consisted of sulfate decomposition at high temperatures and under oxidizing conditions, as well as reductions in sulfate to either sulfide or sulfur dioxide in the presence of reducing agents. The EGA analysis also confirmed emission of CO₂, CO, and O₂.

Xu et al. [13] studied batch reactions and phase transitions of a melter feed in high-level vitrifying of alumina waste at 700 °C via various techniques. Understanding feed-to-glass conversions for vitrification of nuclear waste is also important. Feed is a waste slurry mixture with glass-forming and glass-modifying additives and is charged at the top of the cold cap (the batch blanket) [13, 14].

The purpose of this work is to explain the changes occurring between the nominal and actual chemical compositions of the silicate-phosphate glasses of the SiO₂-P₂O₅-K₂O-MgO-SO₃ system. The actual compositions of the materials were determined by XRF. Changes in the chemical composition were explained by examining the course of the melting process for selected glass batches. The loss of significant amounts of SO₃ from some glasses containing sulfur ions was already mentioned [15]. Although the reasons for significant losses of sulfur during melting of glass batches are well documented in the literature [15, 16], the problem of phosphorus loss is rarely discussed. In this study, EGA was used by coupling with TG/DSC-MS and HT-XRD measurements to investigate batch reactions. When the emphasis on environmental protection is taken into account, it is worth checking the processes and reactions exhibited by the glass batches, especially since these glasses could find application as glassy carriers of sulfur for soil environments.

Materials and methods

Syntheses and chemical compositions of the glasses

A series of sulfur-free and sulfur-containing glasses with nominal compositions $(47-x)\text{SiO}_2 \cdot x\text{P}_2\text{O}_5 \cdot 20\text{K}_2\text{O} \cdot 33\text{MgO}$ and $(47-x)\text{SiO}_2 \cdot x\text{P}_2\text{O}_5 \cdot 20\text{K}_2\text{O} \cdot 28\text{MgO} \cdot 5\text{SO}_3$ ($x = 2, 3, 4, 5, 6, 7, 8, 8.5, 9, 10, 11$ mol.%) were prepared. The starting materials were of analytical grade (> 99% purity), including SiO_2 , $(\text{NH}_4)_2\text{HPO}_4$, K_2CO_3 , MgO , and K_2SO_4 . All batches containing sulfate included activated carbon as a reducer with an amount equivalent to that of the added K_2SO_4 . The raw material mixtures were melted in ceramic crucibles in electric furnaces at 1450 °C in air. The melts obtained were poured onto a steel plate.

The actual chemical compositions of the synthesized glasses were determined by X-ray fluorescence spectrometry (XRF) using a Thermo Scientific ARL Advant'XP spectrometer and normalizing the glass sample composition to 100%. The nominal chemical compositions of the samples in mass percent along with those determined by X-ray fluorescence spectrometry (XRF) are listed in Tables 1 and 2. The glasses were marked in accordance with the molar contents of their individual components expressed as oxides.

Table 1 Nominal and experimental chemical compositions (from XRF analysis) of S-free glass in mass%

Comp	SiO ₂		P ₂ O ₅		K ₂ O		MgO		Al ₂ O ₃	Other*
	Nom	XRF	Nom	XRF	Nom	XRF	Nom	XRF		
Glass name										
45Si2P	43.60	41.94	4.58	5.26	30.38	29.29	21.45	21.26	1.06	1.19
44Si3P	42.07	39.96	6.78	7.77	29.98	28.78	21.17	20.58	1.60	1.31
43Si4P	40.59	38.73	8.92	10.20	29.60	28.17	20.90	20.54	1.15	1.21
42Si5P	39.15	36.85	11.01	12.32	29.22	28.84	20.63	19.24	1.26	1.50
41Si6P	37.73	38.51	13.04	13.81	28.85	22.61	20.37	22.62	0.96	1.49
40Si7P	36.35	33.45	15.03	16.28	28.50	30.18	20.12	16.87	1.37	1.85
39Si8P	35.01	32.45	16.97	18.43	28.15	29.85	19.87	16.99	1.17	1.11
38.5Si8.5P	34.35	29.44	17.92	18.37	27.98	36.26	19.75	12.98	1.78	1.18
38Si9P	33.70	29.67	18.86	19.90	27.81	32.82	19.63	14.34	1.67	1.60
37Si10P	32.42	28.45	20.70	21.74	27.48	32.64	19.94	14.04	1.92	1.21
36Si11P	31.18	28.85	22.50	24.97	27.15	26.82	19.17	16.36	1.56	1.45

*a.o.: Na₂O, CaO, Fe₂O₃, CuO, ZnO

Table 2 Nominal and experimental chemical compositions from XRF analyses of S-bearing glasses in mass%, as well as P₂O₅ and SO₃ losses in %

Comp	SiO ₂		P ₂ O ₅		K ₂ O		MgO		SO ₃		Al ₂ O ₃	Other	P ₂ O ₅ losses	SO ₃ losses
	Nom	XRF	Nom	XRF	Nom	XRF	Nom	XRF	Nom	XRF				
Glass name														
45Si2P5S	42.24	47.00	4.44	2.86	29.43	25.13	17.63	20.01	6.25	2.24	1.43	1.32	35.49	64.12
44Si3P5S	40.78	46.63	6.57	3.49	29.06	25.02	17.41	20.15	6.18	1.74	1.62	1.36	46.95	71.79
43Si4P5S	39.36	45.48	8.65	1.85	28.70	23.53	17.19	20.30	6.10	5.94	1.45	1.45	78.66	2.56
42Si5P5S	37.97	40.36	10.68	8.70	28.35	25.13	16.98	18.11	6.02	4.90	1.39	1.42	18.54	18.71
41Si6P5S	36.62	41.33	12.66	9.77	28.00	23.88	16.77	17.86	5.95	3.96	1.90	1.29	22.81	33.45
40Si7P5S	35.29	39.53	14.59	8.73	27.67	26.37	16.57	18.50	5.88	4.08	1.36	1.44	40.14	30.67
39Si8P5S	34.00	41.09	16.48	8.45	27.34	25.02	16.38	19.33	5.81	3.75	1.09	1.25	48.71	35.41
38.5Si8.5P5S	33.37	38.69	17.40	10.33	27.18	26.46	16.28	18.36	5.77	1.98	2.28	1.91	40.67	65.71
38Si9P5S	32.74	37.70	18.32	11.39	27.02	25.97	16.18	18.42	5.74	2.87	1.78	1.88	37.85	50.03
37Si10P5S	31.51	36.20	20.12	13.05	26.70	26.18	16.00	18.14	5.67	2.58	1.96	1.91	35.13	54.62
36Si11P5S	30.31	35.02	21.88	14.95	26.40	24.59	15.81	18.73	5.61	3.60	1.66	1.45	31.65	35.78

Identification of batch reactions

Differential scanning calorimetry-thermogravimetry-evolved gas analysis by mass spectrometry (DSC-TG-EGA (MS)) combination

Batch reactions were analyzed by simultaneous differential scanning calorimetry-thermogravimetry-evolved gas analysis by mass spectrometry (DSC-TG-EGA (MS)) in synthetic air (50 mL min^{-1}) at a heating rate of $10 \text{ }^\circ\text{C min}^{-1}$ using a Simultaneous Thermo Analyzer (STA) [TG-DSC, Netzsch STA 449 F5 Jupiter] coupled to a 403 D Aëolos mass spectrometer. An empty $\alpha\text{-Al}_2\text{O}_3$ crucible was used as the reference substance. For evaluations, 10 mg of dried sample was heated from 37 to $1100 \text{ }^\circ\text{C}$ in a corundum crucible.

High-temperature X-ray diffraction (HT-XRD)

Phase compositions were analyzed during heating of glass batches with X-ray diffraction (XRD), which was performed with a Panalytical Empyrean diffractometer in the range $10\text{--}100 \text{ deg}$. $\text{Cu K}\alpha$ radiation was used, and the detector was a PIXcel3D. High-temperature X-ray diffraction (HT-XRD) measurements were performed up to $1100 \text{ }^\circ\text{C}$ by heating in air with temperature steps of $50 \text{ }^\circ\text{C}$. An Anton Paar HTK 1200 N oven chamber was mounted on the diffractometer for these studies. The crystalline phases were interpreted using HighScore Plus software.

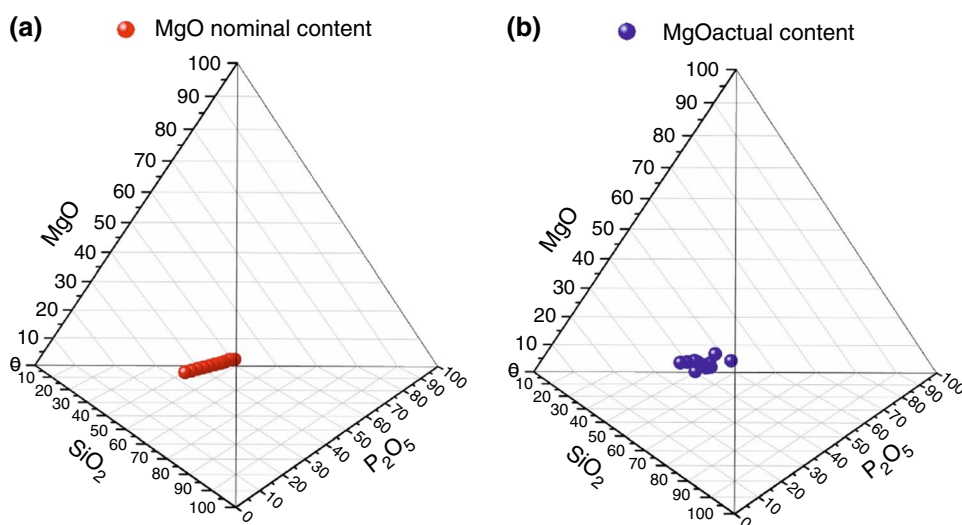
Results

Glass chemical composition

As mentioned above, the nominal chemical compositions of the glasses along with those determined with X-ray fluorescence spectrometry (XRF) for sulfur-free and sulfur-bearing glassy materials are listed in Tables 1 and 2, respectively. Figure 1a and b show, in a very general way (graphically in the form of a 3D tetrahedral plot), the nominal and actual chemical compositions (from XRF analysis) of sulfur-free glassy materials, that is, nominally from the four-component system $\text{SiO}_2\text{-P}_2\text{O}_5\text{-K}_2\text{O-MgO}$. Some of the glass chemical compositions, expressed in mole percentages, have already been presented [17].

Analyses of chemical compositions by XRF showed that glasses containing sulfur were characterized by a reduced P_2O_5 content. The losses of P_2O_5 for all sulfur-bearing glasses were calculated and are presented in Table 2 and Fig. 2a. The P_2O_5 losses did not apply to S-free glasses. In the case of glasses without sulfur ions, the P_2O_5 content was even slightly higher than the nominal value (Table 1). Thus, it is concluded that the loss of this component is related to the presence of potassium sulfate (VI) in the glass batch and, most of all, to the activated carbon acting as a reducing agent. The losses from sulfur-containing glasses as SO_3 are also shown in Table 2 and Fig. 2b. In general, the trend shows that as less sulfur was incorporated into the glass structure, lower losses of P_2O_5 were observed during smelting (Figs. 2). XRF analysis showed that 43Si4P5S glass (Table 2, Fig. 2a) showed the highest loss of P_2O_5 . XRF also showed that the lowest SO_3 loss was recorded during melting of this glass (Table 2, Fig. 2b).

Fig. 1 Approximate 3D tetrahedral presentation of the chemical compositions of the S-free glasses from XRF analyses; **a** nominal and **b** experimental



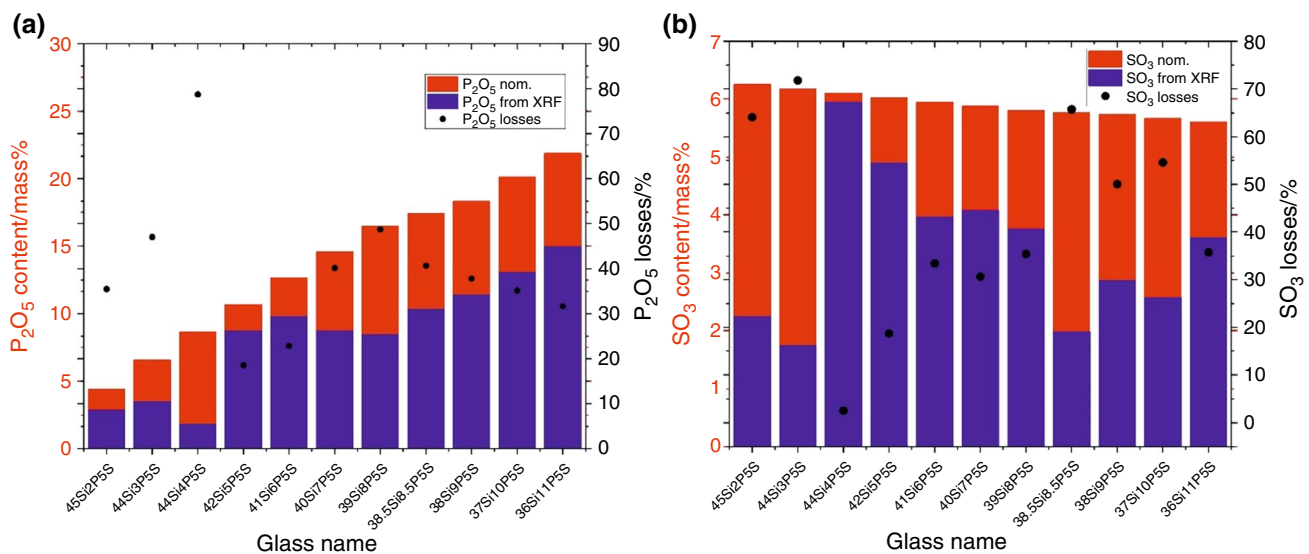


Fig. 2 Chemical composition for each glass containing sulfur ions: **a** nominal and experimental P_2O_5 content/mass% and P_2O_5 losses/%; **b** nominal and experimental SO_3 content/mass% and SO_3 losses/%

It should also be noted that addition of sulfur ions increased the ability to form glasses from the SiO_2 - P_2O_5 - K_2O - MgO system obtained under reducing conditions; therefore, all sulfur-containing materials, according to the XRD analysis, were amorphous, while materials with the highest P_2O_5 content were glass-crystalline materials. The XRD results were partially shown in a prior report [17]. However, it was decided to focus on the materials constituting the subject of the work, including the 43Si4P, 43Si4P5S, and 36Si11P5S glasses.

Identification of batch reactions

DSC-TG-EGA (MS) results

Three selected glass batches, 43Si4P, 43Si4P5S, and 36Si11P5S, were subjected to differential scanning calorimetry-thermogravimetry-evolved gas analysis by mass spectrometry (DSC-TG-EGA (MS)) to determine their behavior during heating.

The potassium sulfate (VI) and activated carbon contained in the 43Si4P5S glass batch were specifically chosen for EGA by a coupled TG/DSC-MS study due to significant differences between the nominal and XRF chemical compositions (Table 2). Additionally, the 43Si4P glass batch was chosen as an analog of this sulfur-containing 43Si4P5S glass batch.

The DSC-TG curves obtained for the three selected glass batches 43Si4P, 43Si4P5S and 36Si11P5S during heating of the samples are presented in Fig. 3. The DSC-TG-EGA (MS) curves for 36Si11P5S, 43Si4P5S, and 43Si4P are shown in Figs. 4, 5, and 6, respectively.

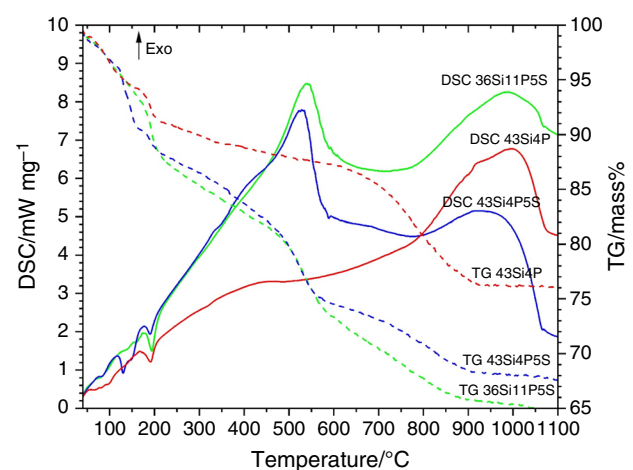


Fig. 3 DSC and TG curves for all glass batches studied

The profiles of the DSC-TG curves (Fig. 3) indicated that heating the glass batches up to 1100 °C occurred in several stages. Some steps were difficult to separate because of overlapping features in the DSC-TG curves. The heating steps are listed in Table 3 for the 36Si11P5S and 43Si4P5S glass batches and in Table 4 for the 43Si4P glass batch.

According to the literature, hygroscopic water was released at temperatures of 100–130 °C. Dehydration occurring below 110 °C was associated with weak binding of water molecules [18].

The TG curves confirmed that the mass losses occurring at temperatures up to 200 °C were caused by losses of hygroscopic water (the first mass loss recorded on the TG curve) and water from decomposition of diammonium

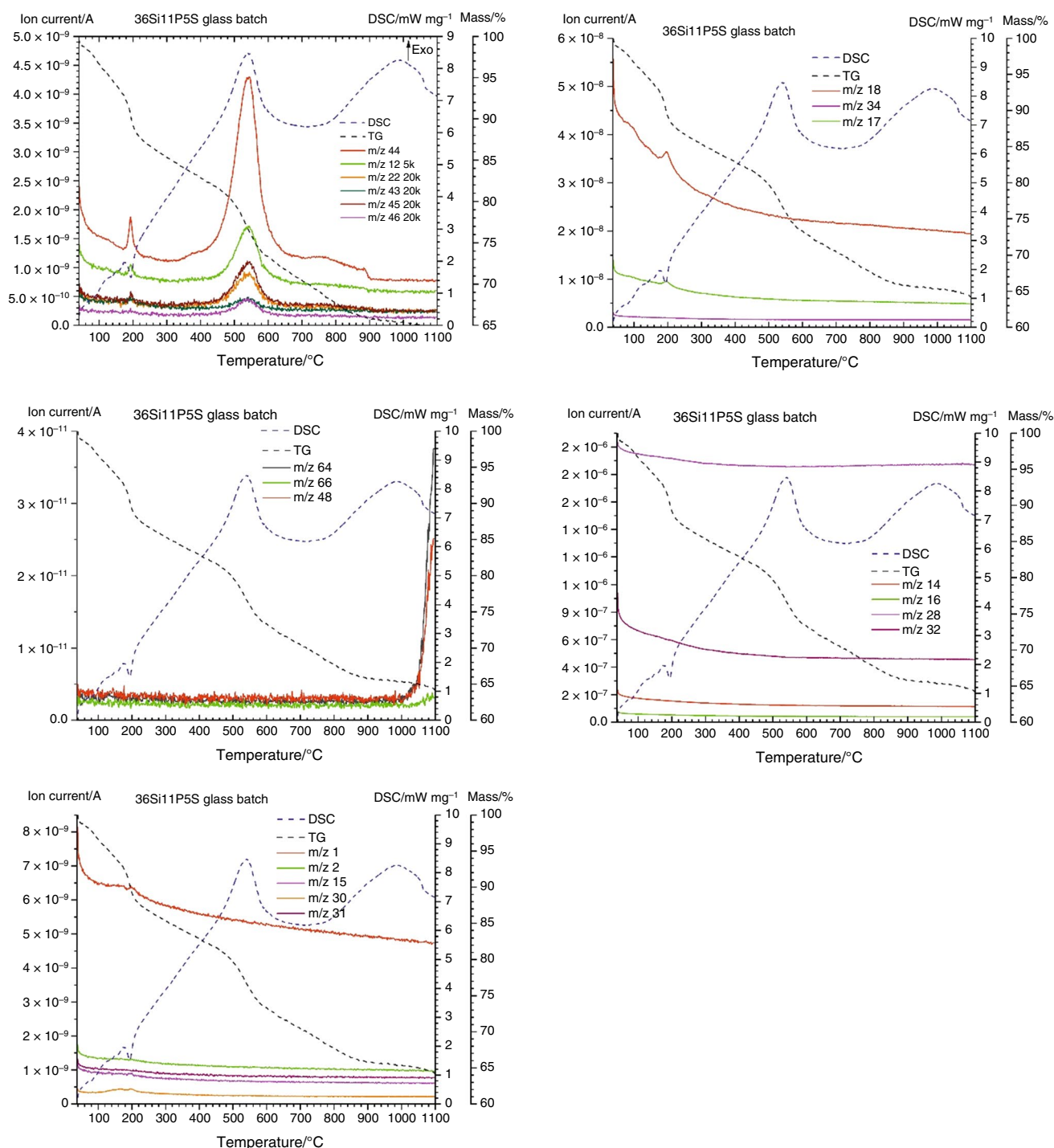


Fig. 4 DSC-TG-EGA (MS) curves for the 36Si11P5S glass batch

hydrogen phosphate ($(\text{NH}_4)_2\text{HPO}_4$). At a temperature of approximately 200 °C, there was a decrease in mass due to evolution of ammonia NH_3 [19]. It is not easy to distinguish the signals for the decomposition products of ammonium hydrogen phosphate because of the overlap of these reactions.

Subsequently, the DSC curve showed a very pronounced exotherm related to evolution of CO_2 , which came from combustion of activated carbon in glass batches also containing K_2SO_4 (36Si11P5S and 43Si11P5S glass batches), and this was accompanied by a decrease in mass. Another mass loss recorded on the TG curve was related to decomposition of

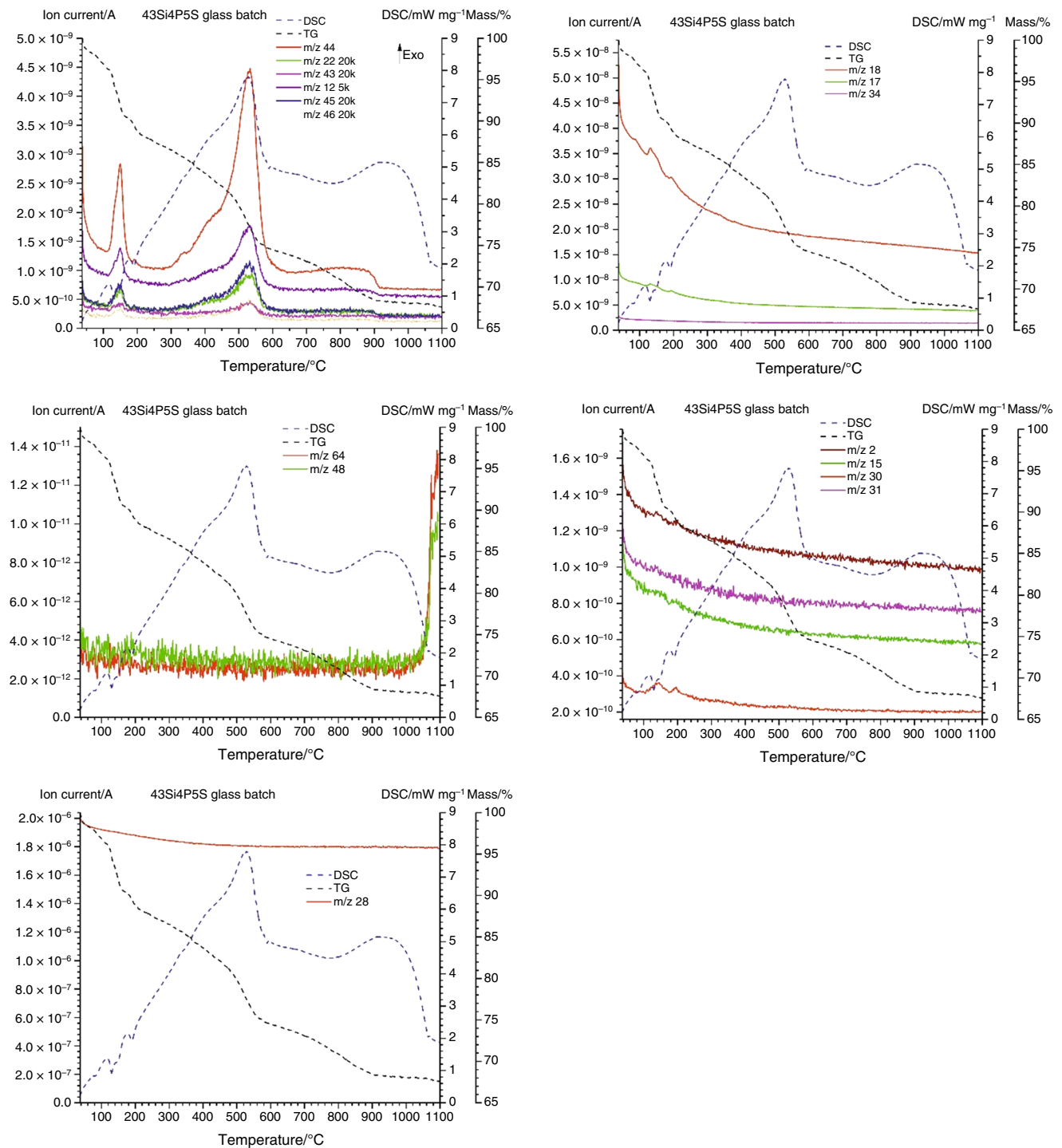


Fig. 5 DSC-TG-EGA (MS) curves for the 43Si4P5S glass batch

K_2CO_3 , which also caused the release of CO_2 , and this phenomenon occurred with all glass batches studied. However, the changes in mass due to thermal decomposition of K_2CO_3 gave weak endothermic features on the DSC curves. Furthermore, this weak endothermic effect was superimposed on the

exothermic effect for combustion of activated carbon in the glass batches containing sulfate.

Based on the TG curves, it was concluded that the total mass losses from glass batches containing K_2SO_4 , e.g., 36Si11P5S and 43Si4P5S, were 33 and 31%, respectively.

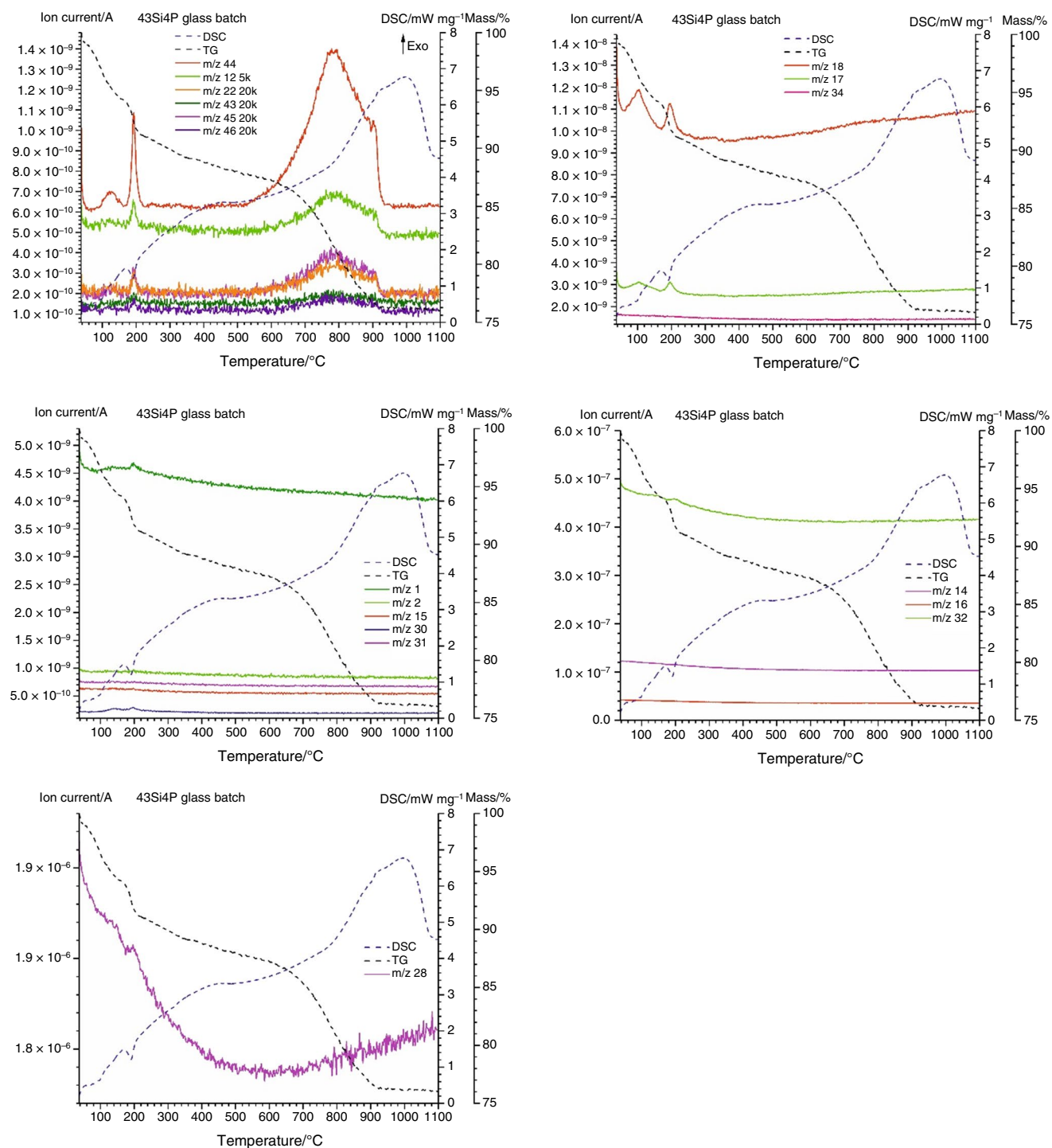


Fig. 6 DSC-TG-EGA (MS) curves for the 43Si4P glass batch

For identification of the gaseous product produced during heating of the studied glass batches, the ion currents for the key masses, which were represented as mass-to-charge ratios, m/z , were measured. Based on prior literature, the following was measured:

- Gaseous forms of sulfur: SO_2 (m/z 48); SO_3 (m/z 64, main mass; and m/z 66, isotopologue [20] [21]); H_2S (m/z 34); HSO_4^- (m/z 97); K_2SO_4 (m/z 174) [22] for sulfur-containing glass batches;

Table 3 Thermogravimetric and DSC analyses of 36Si11P5S and 43Si4P5S glass batches

Stage	36Si11P5S			43Si4P5S		
	DSC T _{peak} /°C	TG temp. range /°C	TG Δm /%	DSC T _{peak} /°C	TG temp. range /°C	TG Δm /%
I	81	37–118	4.2	85	37–114	3.8
II	136	118–153	1.8	132	114–141	2.8
III	160	153–178	1.1	151	141–167	2.5
IV	193	181–225	4.6	190	167–211	2.2
V	540	220–595	14.3	525	211–566	13.2
VI	590	–	–	589	–	–
VII	n.s.*	595–869	7.2	n.s.	566–911	6.8
VIII	987	–	–	983	–	–

*n.s.—Not specified

Table 4 Thermogravimetric and DSC analyses of the 43Si4P glass batch

Stage	43Si4P		
	DSC T _{peak} /°C	TG Temp. range /°C	TG Δm /%
I	83	37–155	5.7
II	98	–	–
III	192	155–221	3.2
IV	n.s.	221–926	14.8
V	998	–	–

*n.s.—Not specified

- The compounds containing phosphorus were measured with the indicated m/z values: P₂ (m/z 62); P₄ (m/z 124); PO (m/z 46); PO₂ (m/z 63); P₂O₅ (m/z 142); P₄O₁₀ (m/z 284); P₂O₃ (m/z 110) and P (m/z 31), as noted in the literature [23, 24];
- The mass spectra for carbon compounds were also measured as the glass batch contained activated carbon as well as K₂CO₃ to produce C (m/z 12); O₂ (m/z 32); O⁺ (m/z 16); CO₂²⁺ (m/z 22); CO₂ (m/z 44, main mass 45–49) and CO (m/z 28) [25];
- Other gaseous species, including H (m/z 1 and 2); N⁺ (m/z 14); NO (m/z 30); NH⁺ (m/z 15); NH₂⁺ (m/z 16); NH₃⁺ (m/z 17) and NH₄⁺ (m/z 18) [26], were also measured.

Figures 4, 5, and 6 show only the ion currents detected in the mass spectra; therefore, only these are considered in this work.

Evolution of water vapor

As indicated by the EGA curves, water was released. Furthermore, the ion scans performed in the mass spectrometer at temperatures of 37–200 °C showed signals at m/z 17 and 18 (Figs. 4–6) related to the OH⁺ and H₂O⁺ species [18, 27,

28]. Therefore, water evolved from the batch, based on the EGA curves.

Diammonium phosphate decomposition

According to the literature [21], five of the most intense peaks for ammonia occur at m/z 17 (100% relative intensity), 16 (80%), 15 (7%), and 14 (2%), and with the lowest intensity peak is at m/z 18 (0.4%). When the glass batches were heated, the diammonium hydrogen phosphate decomposed, and the peaks derived from NH₃⁺ and OH⁺ overlapped each other. The very small signals for m/z 16, 15, and 14 were also recorded in the EGA spectra for the glass batches.

The signal at m/z 30 in the spectrum may be related to NO that was produced by oxidation of the NH₃ produced from decomposition of diammonium hydrogen phosphate. However, according to the literature, NO emissions occur at higher temperatures (400–600 °C) [18], so this assignment is rather unlikely.

Evolution of CO₂

The evolution of carbon as CO₂ is shown in Figs. 4–6. Sources of CO₂ included the background in the EGA data, oxidation of organic products, and decomposition of carbonates (the research carried out indicates decarbonization of K₂CO₃). Lewis et al. [29] made similar observations.

According to the literature [30], CO₂ ions appears at m/z 44 through m/z 49.

In the analyzed glass batches, EDS spectra were recorded for m/z ratios of 44, 45, and 46, but spectra for m/z 47, 48, 49 were not recorded. Santrock et al. [30] concluded that, with the exception of m/z 44 (¹²C¹⁶O¹⁶O), all measurable ion currents represented sums of multiple isotopic contributions (¹³C¹⁷O¹⁶O + ¹²C¹⁸O¹⁶O + ¹²C¹⁷O₂ at m/z 46; ¹²C¹⁷O¹⁶O + ¹³C¹⁶O¹⁶O at m/z 45). Mass spectrometers used to analyze CO₂ register three common ion beam currents corresponding to m/z 44, 45, 46, which comprise various

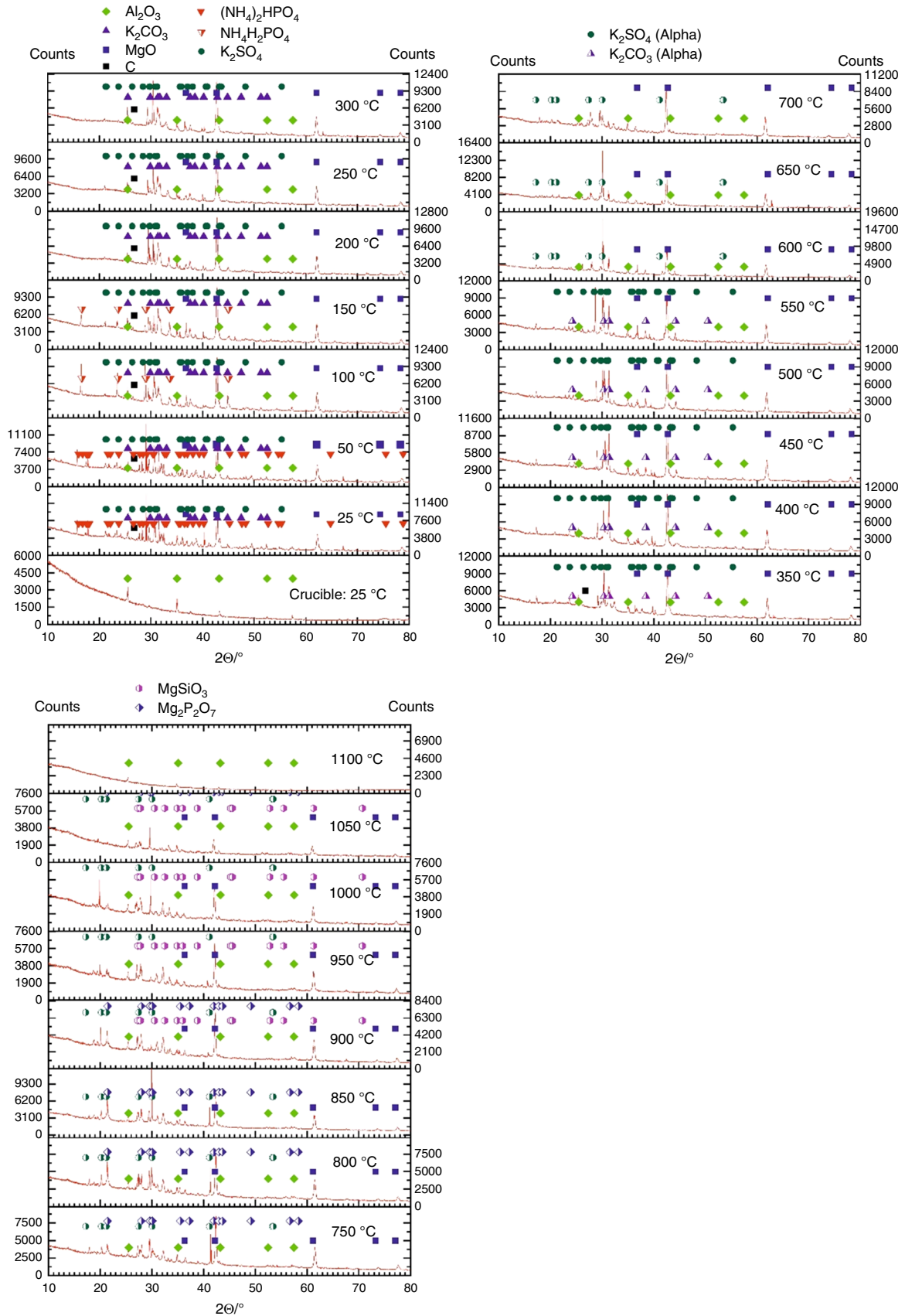


Fig. 7 Powder HT-XRD patterns for the 43Si4P5S glass batch during heating from 25 to 1100 °C and for the crucible at 25 °C. X-ray diffractometry (XRD) identification of phases (MgO, Al₂O₃, (NH₄)₂HPO₄, NH₄H₂PO₄, K₂CO₃, K₂SO₄, MgSiO₃, Mg₂P₂O₇)

isotopomers. The most abundant ¹²C¹⁶O¹⁶O molecule is recorded at *m/z* 44 and was registered in the presented study.

In this study, EGA spectra were also recorded for *m/z* 45 and 46. According to the literature [30] on *m/z* 45, the ¹³C-containing isotopologue is dominant, while the ¹⁷O-containing isotopologue contributes only ~6.5%. In the case of *m/z* 46, an ¹⁸O-bearing isotopologue prevails because doubly substituted molecules have much lower abundances. No further CO₂ isotopologues were registered in this research; that is because double or triple substitutions have very low abundance; CO₂ has double and triple isotopologues with *m/z* ratios from 47 to 49, but they have low abundance and were not registered.

The ion current tracks corresponding to *m/z* 22 were connected to CO₂²⁺ (Figs. 4–6). In an earlier study, [28] evaporation of CO₂²⁺ and CO²⁺ (*m/z* 44) occurred in the temperature range 200–249 °C.

Furthermore, in the mass spectra, more signals associated with evolution of CO₂ were observed. It must be noted that one of the main fragment ions formed was CO⁺ (*m/z* 28). This testified to the presence of carbon monoxide in the gaseous products from the glass batch. MS peaks were also registered for ion fragments with *m/z* = 12 (C⁺) [8, 25, 31]. The very weak spectrum recorded for *m/z* = 16 was assigned to the presence of atomic oxygen (O⁺), which is also a fragment from the released gases CO and CO₂ [8, 31].

Thermal decomposition of K₂SO₄

In the EGA curves for glass batches containing potassium sulfate (VI) and activated carbon (36Si11P5S and 43Si4P5S), signals arose from SO₂ (*m/z* 48) and SO₃ (*m/z* 64) but only at temperatures above 1000 °C. In the case of the 36Si11P5S glass batch, a signal was also recorded for *m/z* 66, that is, for an isotopologue of SO₂.

High-temperature X-ray diffractometry (HT-XRD)

The 43Si4P5S and 43Si4P glass batches heated to 1100 °C were analyzed with high-temperature X-ray diffraction (HT-XRD). The diffractograms obtained are shown in Figs. 7 and 8 for 43Si4P5S and 43Si4P, respectively.

43Si4P5S glass batch

The diffractograms obtained at every 50 °C from the HT-XRD measurement of the 43Si4P5S glass batch heated from 25 to 1100 °C are shown in Fig. 7. The figure also

shows the diffractogram measured at 25 °C for the empty crucible in which the measurements were carried out, which indicated the presence of an Al₂O₃ phase in the analyzed samples.

The diffraction pattern obtained at 25 °C revealed the components of the glass batch (Fig. 7). Thus, crystalline phases of (NH₄)₂HPO₄, MgO, K₂CO₃, K₂SO₄, and Al₂O₃ from the crucible in which the HT-XRD measurement were identified (SiO₂ was amorphous).

The diffractogram recorded at 50 °C (Fig. 7) was similar in appearance to that recorded at 25 °C; therefore, in this case, all the components introduced in the 43Si4P5S glass batch were identified.

The diffraction pattern recorded at 100 °C differed from the diffraction patterns obtained at 25 and 50 °C because new peaks appeared and some of those present in the diffraction patterns recorded at lower temperatures disappeared. In this case, the peak for (NH₄)₂HPO₄ disappeared, and the product of its decomposition, i.e., (NH₄)H₂PO₄, began to appear.

The diffractogram recorded at 150 °C differed from the others because some of the phases seemed to disappear. At a temperature of 150 °C, the glass batch must still contain SiO₂, K₂CO₃, MgO, and K₂SO₄. Theoretically, NH₄H₂PO₄ (ICDD: 00–037–1479) was also present.

The diffraction pattern for the glass batch heated at 200 °C showed increased intensity for the peak with a 2θ value of approximately 30° compared to that for the diffraction pattern recorded at 150 °C.

The diffractogram recorded at 300 °C generally did not differ in the positions of the reflections, but they differed in intensity. The diffraction pattern recorded at 350 °C did not differ significantly from the diffractogram recorded at 300 °C.

The diffractogram recorded at 400 °C differed from its predecessor within the 2θ range 29 to 33°. This is related to the beginning of the coal combustion process which was also shown in the DSC-TG-EGA (MS) studies (Figs. 4, 5). At temperatures of 450 and 550 °C, there were further changes in this range for the 2θ angles.

The diffractograms recorded at temperatures of 450 and 500 °C were very similar to each other, even in terms of peak locations and intensities. This means that in this temperature range, there were no changes in the batch. At 550 °C, there were changes in the 2θ angles within the range 29 to 33°.

At 600 °C, significant changes in phase composition took place in the sample, which were indicated by a significant decrease in the intensity of the peaks at approximately 29° and approximately 31.5°. The diffractogram for the 43Si11P5S glass batch recorded at 650 °C differed from that recorded at 600 °C due to decreases in the intensities of the reflection peaks. At 700 °C, there were large changes in the peaks between 29 and 33°.

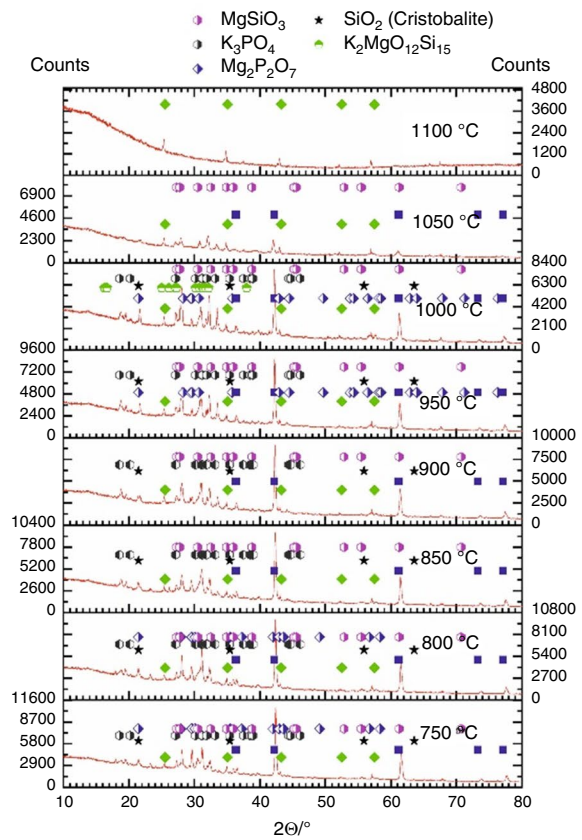
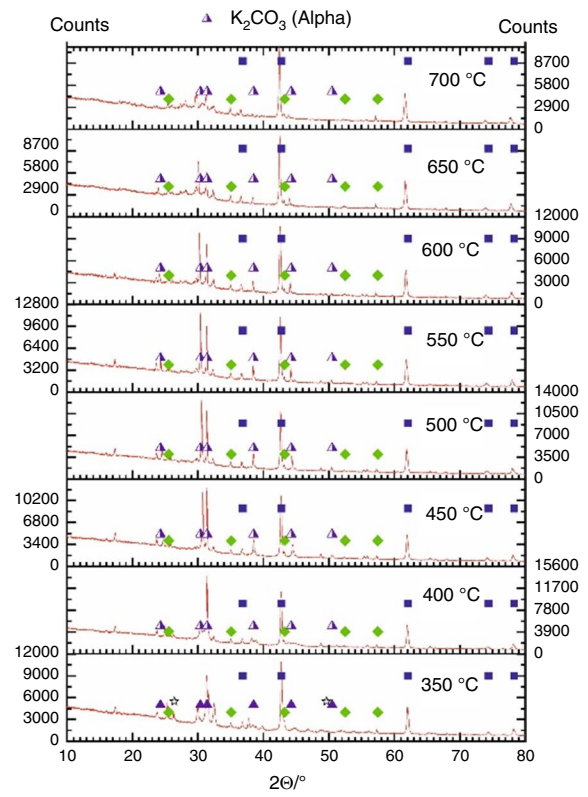
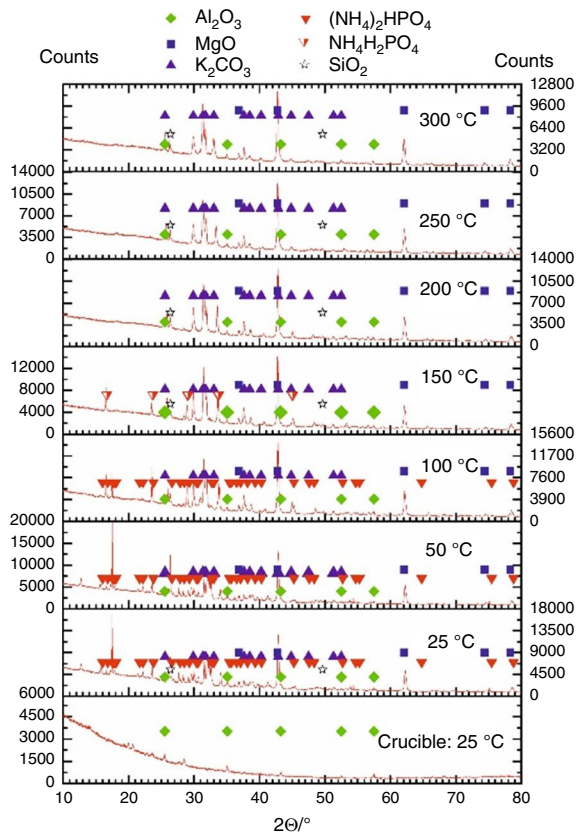


Fig. 8 Powder HT-XRD patterns for the 43Si4P glass batch during heating from 25 to 1100 °C and for the crucible at 25 °C. X-ray diffractometry (XRD) identification of phases (MgO, Al₂O₃, (NH₄)₂HPO₄, NH₄H₂PO₄, K₂CO₃, MgSiO₃, K₃PO₄, SiO₂, K₂MgO₁₂Si₅)

As shown by the XRD analyses, the diffraction patterns still showed clear reflections indicating the presence of MgO, and the intensity gradually decreased up to a temperature of 1050 °C. In the temperature range 750 to 1050 °C, peaks for new crystallization phases were evident. Most likely, they were for magnesium silicate, MgSiO₃ (ICSD: 98-003-1288), and phosphates such as Mg₂P₂O₇ (ICSD: 98-001-5326).

At a temperature of 1100 °C, the diffraction pattern for the 43Si4P5S glass batch showed only Al₂O₃ reflections (the crucible material) because, under the measurement conditions used, it is probable that a silicate phase was produced, quartz grains were dissolved in the melt, and a glass was formed.

43Si4P glass batch

Diffractograms for the 43Si4P glass batch were also analyzed (Fig. 8).

The lack of K₂SO₄ and the addition of activated carbon to the 43Si4P glass batch caused obvious differences in its HT-XRD diffractograms compared to the diffractogram for the 43Si4P5S glass batch that contained K₂SO₄.

When this glass batch was heated to 1100 °C, as with the corresponding sulfur-containing glass batch (43Si4P5S), only peaks derived from Al₂O₃ and originating from the crucible appeared in the diffraction pattern (Fig. 8).

In contrast to the diffractogram for the 43Si4P5S glass batch (Figs. 7, 8), the diffractogram recorded at 750 °C for the 43Si4P glass batch showed crystal phases such as MgO (ICSD: 98-015-7526), SiO₂ (cristobalite high, ICSD: 00-027-0605), MgSiO₃ (Protoenstatite, ICSD: 98-003-1288), Mg₂P₂O₇ (ICSD: 98-003-1288), and K₃PO₄ (ICSD: 98-015-8801).

At a temperature of 1000 °C, the presence of MgSiO₃ (ICSD: 98-003-1288), Mg₂P₂O₇ (ICSD: 98-003-1288), and K₂MgO₁₂Si₅ (ICSD: 98-007-4571) crystalline phases was also identified.

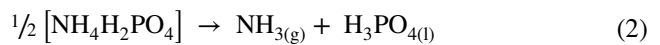
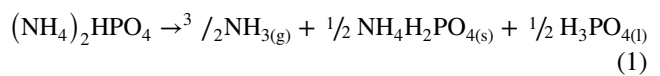
The diffractogram for the sulfur-free glass batch (43Si4P) differed from that for its counterpart containing K₂SO₄ and activated carbon. The crystalline phases identified in the 43Si4P glass batch were, MgO (Periclase, ICSD: 98-015-9373), MgSiO₃ (ICDD: 01-074-2017), SiO₂ (Cristobalite high, ICSD: 00-027-0605), Mg₂P₂O₇ (ICSD: 98-003-1288), and Al₂O₃ (ICSD: 98-016-0607).

Discussion

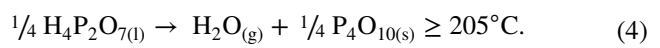
As part of this study, the formation of glasses in batches comprising SiO₂, (NH₄)₂HPO₄, K₂CO₃, MgO, K₂SO₄, and activated carbon, i.e., 43Si4P5S and 36Si11P5S, was investigated, as was the glass batch 43Si4P that did not contain potassium sulfate and activated carbon.

There is no doubt that when the glass batches were heated, waters of hydration evaporated. At temperatures of 100–130 °C, water was released. However, for the glass batches under consideration, decomposition of (NH₄)₂HPO₄ also occurred. One of the decomposition products was water, and ammonia was another important decomposition product.

At low temperatures [19], ammonia was released according to the following reactions:



this led to the formation of phosphoric acid. The acid was dehydrated as in the reaction below, producing pyrophosphoric acid [19]



This reaction proceeded at a very slow rate with formation of P₄O₁₀. Immediately [19] after formation, P₄O₁₀ sublimed at 579 °C.

Due to the m/z peak at 18 for NH₄⁺, it overlapped with the peak for H₂O.

It seems that the above reactions are consistent with the glass batches under study.

Based on the results of their EGA study, Rodriguez et al. [14] stated that TG peaks below 400 °C corresponded mainly to evolution of H₂O and even H₂O release at temperatures above 400 °C when CO₂ was already released. However, they did investigate gas-evolving cold-cap reactions, and chemically bonded water was also included among the ingredients. In this work, H₂O may also have been produced by (NH₄)₂HPO₄ decomposition, as mentioned above.

In the recorded DSC curves for the 43Si4P and 36Si11P5S glass batches, a very weak endothermic effect was observed at temperatures above 573 °C, which was related to transformation of β-quartz into α-quartz. This transformation was not visible in the DSC curve for the 43Si4P5S glass batch, but such a transformation had to take place.

As mentioned before, the DSC peaks for individual gases overlapped. Rodriguez et al. [14] also observed overlap in their study on the composition of melt feeds used to vitrify high-level waste containing high alumina content

in the preparation of glass containing the minerals SiO_2 , Al_2O_3 , B_2O_3 , Na_2O , CaO , Fe_2O_3 , Li_2O , Bi_2O_3 , and P_2O_5 .

Certainly, in the case of the glass batches studied herein, there was overlap between peaks on the DSC curve for the exothermic effect associated with carbon combustion and the endothermic effect associated with thermal dissociation of K_2CO_3 . Both of these processes led to release of CO_2 . The CO_2 emitted from the glass batch was very evident from the TG, EGA and DSC curves, and it occurred within the range 400 to 800 °C and even below 200 °C. It was noticed that below 550 °C, large amounts of CO_2 gas were released, while above this temperature, the amount of released gases decreased dramatically.

The EGA curves for the 36Si11P5S and 43Si4P5S glass batches (Fig. 4, 5) showed three peaks (effects), the first of which was related to CO_2 emission from combustion of activated carbon:



and the second was related to CO_2 emission from decomposition of K_2CO_3 , as in the following reaction:



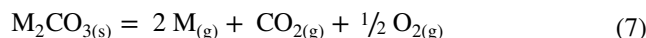
Kloužek et al. [32] showed the gases evolved from a mixture containing sulfate (0.20 mass% SO_3), granulated coke (0.05 mass%) and glass cullet. Other raw materials were not used in their work, as CO_2 formed by decomposition of carbonates would have overlapped the peaks for gases produced by the reactions studied. Kloužek et al. [32] observed oxidation of carbon by oxygen (Eq. 5) at a low temperature of 350 °C.

As reported by Tsujimura et al. [33], small amounts of CO_2 were released up to 200 °C, probably due to CO_2 absorption from the atmosphere on the batch surface.

Lehman et al. [34] studied the behavior of potassium carbonate near its melting point with thermal analysis and at a total pressure of 1 atm. Therefore, they investigated the specific behavior of K_2CO_3 between 700 and 1000 °C and under various partial pressures of CO_2 . K_2CO_3 occurs in two forms, γ and β . As previously reported [34], the γ phase transforms to the β form at 421 °C, and the β form is stable up to the melting point, which is close to 900 °C. Carbonate thermally decomposes at high temperature according to the reaction in Eq. 5.

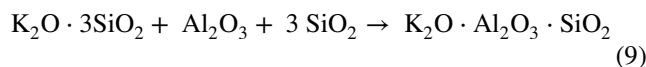
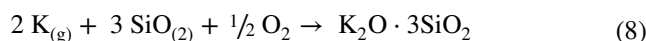
Lehman et al. [34] also observed, with thermogravimetric analyses, that substitution of CO_2 for N_2 reduced the rate of volatilization, but measurable mass losses still occurred at all temperatures. Based on the temperature and partial pressure dependence of CO_2 mass losses, the results supported a K_2CO_3 decomposition model rather than a congruent sublimation/evaporation model.

Sergeev et al. [7] analyzed vaporization of the alkali carbonates Na_2CO_3 and K_2CO_3 by Knudsen diffusion mass spectrometry within the temperature range 600 to 880 °C. It was established that sodium and potassium carbonates evaporated congruently below 750 °C according to the following reaction:



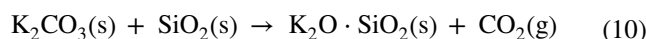
This research [7] showed that at higher temperatures, $p(\text{CO}_2)$ increased disproportionately relative to $p(\text{M})$ in both cases ($\text{M}=\text{Na}$ and K), which led to formation of M_2O oxides in the solid phase. It was established that vaporization of sodium and potassium carbonates was close to congruent at temperatures below 750 °C with the main species M , CO_2 , and O_2 formed in the gas phase. At temperatures higher than 750 °C, incongruent vaporization was observed due to a disproportionate increase in the vapor pressure of CO_2 . At this stage, Na_2O^+ , K_2O^+ , and K_2CO_3^+ ions were also registered in the mass spectra. However, in our work, we did not investigate evaporation of K_2CO_3^+ ions.

If gaseous potassium were present among the gaseous products, Huang et al. [35] indicated it would react with SiO_2 in the presence of O_2 . Huang et al. [35] concluded that in the presence of O_2 , K compounds may react with SiO_2 or Al_2O_3 to form insoluble aluminosilicates, such as $\text{K}_2\text{O} \cdot \text{Al}_2\text{O}_3 \cdot \text{SiO}_2$, via the following equations:



K_2CO_3 , as with other alkaline carbonates and earth-alkaline carbonates, decomposed due to the increase in temperature, that is, thermal calcination occurred above a certain temperature, or through reaction with other batch constituents, that is, reactive calcination. Thermal calcination of K_2CO_3 occurred via Eq. 6 [36]:

Reactive calcination of K_2CO_3 may have resulted from a solid-state reaction with silica that formed a crystalline potassium silicate phase. Formation of potassium metasilicate ($\text{K}_2\text{O} \cdot \text{SiO}_2$) due to reactive calcination of K_2CO_3 with silica is given by:



The following [3] considered reactive calcination of carbonates. Huang et al. [35] also proposed the above reaction.

In fact, none of the DSC curves showed any endothermic effect related to release of CO_2 resulting from thermal decomposition of K_2CO_3 , but this decomposition certainly occurred because a mass loss was registered in the TG data.

Stern and Weise [36] also studied thermal decompositions of K_2CO_3 up to a temperature of 1100 K (827 °C).

No further measurements of decomposition pressures were obtained because data for K_2O are lacking above this temperature. K_2O is sufficiently unstable toward dissociation to $K(g)$ and O_2 to be significant.

As noted by Stern and Weise [36], K_2CO_3 also showed a phase change, and at 523 K (250 °C), the transformation of phases c and IV into phases c and II took place; at a temperature of 701 K (428 °C), the transformation of phases c, III, wc, and II took place; at a temperature of 895 °C, the transformation of phases c, II, wc and I took place; and at a temperature of approx. 1171 K (898 °C), phases c and I transformed into a liquid.

When considering the course of a reaction for sulfate-containing glass batches, the Boudouard reaction should be mentioned. According to the reaction mechanism described by Boudouard [37] of the glasses, released CO partially reacts with the activated carbon added to the batch as a reducing agent according to the reaction equation:



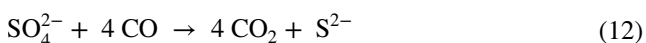
The Boudouard reaction generates a large volume of CO throughout the batch blanket, typically between 670 and 930 °C (940–1200 K) [37].

Evolution of CO was observed between 650 and 1000 °C and paralleled the release of CO_2 formed by decomposition of carbonates. SO_2 evolved at temperatures between 850 and 1350 °C in prior work [5].

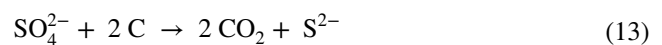
Under reducing conditions, C and CO reduced sulfate ions to sulfide ions or SO_2 gas. CO production required the presence of CO_2 from reactions of the batch. The sulfides produced provided the potential for subsequent reactions with their sulfate precursors [37]. Both sulfate-reducing reactions (involving carbon compounds or sulfides) produced SO_2 .

According to [9], thermal decomposition of the sulfates (in their case Na_2SO_4) added to soda-lime-silica glasses occurred at temperatures greater than 1450 °C, and the SO_2 and O_2 gases were released in a 2:1 ratio from glass batches without a reducing agent added. For the glass batches considered herein, decomposition of potassium sulfate occurred at temperatures above 1000 °C.

According to Vernerova et al. [15], the peak for CO generated at 900 °C indicated the occurrence of the Boudouard reaction between gaseous CO_2 from the batch carbonates and solid carbon. The presence of CO signals the expected reduction in sulfate to sulfide in the temperature range 900–1000 °C:

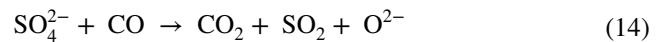


Participation of the reaction with carbon is also anticipated at slightly lower temperatures:

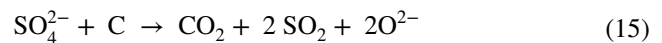


The effect of either reaction depends on the amount of CO_2 available for the Boudouard reaction and the chance that the reactants come into contact [15].

Subsequent reduction in the sulfates to SO_2 was apparent between 1040 and 1200 °C, with the maximum rate occurring at 1090 °C [15]:



A reaction with carbon seems to be probable as well, depending on the content of carbon in the melt, owing to the very low concentration of CO [15].



The sulfur content was also much lower than that assumed for the glasses produced. The structures of the S-bearing glasses contained reduced forms of sulfur, probably from reduction in potassium sulfate with activated carbon in accordance with the equations presented above. The presence of reduced sulfur in the structures of glasses with similar chemical compositions was shown in an earlier publication [38].

During low-temperature heating, orthorhombic K_2SO_4 undergoes a phase transition to high-temperature hexagonal K_2SO_4 at 586 °C [39]. According to the literature, the melting point of K_2SO_4 is 1069 °C [22]. Therefore, in the sulfur-containing glass batches analyzed here, potassium sulfate should decompose because the measurements were carried out up to 1100 °C with the use of HT-XRD. Therefore, results obtained indicated that potassium sulfate must have begun to decompose, as seen from the EGA curves.

Our observations from the EGA curves showed that addition of activated carbon did not reduce the temperature of K_2SO_4 decomposition.

According to the literature [40], retention of sulfates or the total retention of sulfur after batch melting depended strongly on the presence of organic components or coke in the batch. Some SO_2 will be released due to reactions between sodium sulfate (or calcium sulfate) and sand. Taking this into account, it could be concluded that in the case of the glass batches containing potassium sulfate, some SO_2 could be released as a result of a reaction between K_2SO_4 and SiO_2 .

Depending on the batch redox state (determined by reducing and oxidizing components), freshly molten glass could contain SO_4^{2-} , SO_3^{2-} , and S^{2-} , but the composition of this melt may not be uniform (homogeneous).

In the case of the glass batches that contained sulfate, we recorded SO_3 emissions but did not observe sulfate release. Wang et al. [22] did not detect sulfates or SO_3 among the gaseous species, clearly because SO_3 can easily

decompose to SO_2 at high temperature, and the conversion of SO_2 to SO_3 is slow even at temperatures higher than $1000\text{ }^\circ\text{C}$ and usually requires catalysts such as Fe_2O_3 and V_2O_5 [22, 41].

Phosphorus can be volatilized in the following four forms: P_2 , P_4 , PO , and PO_2 . J. Jin et al. [23] noted that volatile phosphorus phases in the temperature range ($1150\text{--}1257\text{ }^\circ\text{C}$) were mainly P_2 and P_4 gases upon reduction by coal.

It is very difficult to say where the significant P_2O_5 losses originated for the glasses studied. Bourgel et al. [24] studied the behavior of phosphorus during gasification of sewage sludge to understand its volatilization conditions during thermal treatments. The authors concluded that volatilization of element P began at $700\text{ }^\circ\text{C}$ when the amount of P_2O_5 was greater than 33 mass%. It increased to 11.5% for 46 mass% of P_2O_5 . Higher temperatures led to greater proportions of P in the gas phase. At $1500\text{ }^\circ\text{C}$, volatilization began at 25 mass% P_2O_5 and reached 55.5% volatilization. At the working temperature (approximately $1300\text{ }^\circ\text{C}$), evaporation began for 25% P_2O_5 content by mass. The composition containing 46 mass% P_2O_5 released 45% of the initial phosphorus.

In the case of the glasses studied, the peak for $m/z\ 31$ was observed, which could indicate the release of gaseous phosphorus (P^+) among other possibilities.

Boström et al. [42] and Grimm et al. [43] showed that, in general, phosphates of alkali and alkaline earth metals are thermodynamically more stable than sulfates, which are in turn more stable than sulfites, which are in turn more stable than silicates and oxides, respectively. On the other hand, potassium salts are generally more stable than magnesium salts. Billen et al. [44] relied on these findings and recognized the aforementioned relationships as useful general rules for estimating speciation of ash elements, which they studied, and the effects of adding certain components to the ash.

In this work, P_2O_5 was formed via decomposition of diammonium hydrogen phosphate. According to the literature, its melting point is $427\text{ }^\circ\text{C}$, that is, 700 K [45]. Thus, P_2O_5 becomes liquid P_2O_5 . It is not known in what form phosphorus was released during melting of the 43Si4P5S glass batch. Even if the peak at $m/z\ 31$ was derived from P^+ , it had a very weak intensity.

Considering the above, it seems appropriate to explain the loss of phosphorus during decomposition of the glasses; research should be carried out in the temperature range 1100 to $1450\text{ }^\circ\text{C}$.

Measurements of the melting processes for the 36Si11P5S, 43Si4P5S, and 43Si4P glass batches were limited to a maximum temperature of $1100\text{ }^\circ\text{C}$. In future, we plan to extend these studies of changes occurring in glass batches to temperatures above $1100\text{ }^\circ\text{C}$.

Conclusions

Chemical reactions occurring between components in sulfur-bearing silicate-phosphate glass batches were studied with a combination of DSC-TG-EGA (MS) and high-temperature X-ray diffraction (HT-XRD) to clarify the reasons for loss of significant amounts of SO_3 and P_2O_5 from glasses in the $\text{SiO}_2\text{-P}_2\text{O}_5\text{-K}_2\text{O-MgO-SO}_3$ system containing sulfur ions.

It was concluded that the most intense processes leading to the release of phosphorus from glass batches occur at temperatures above $1100\text{ }^\circ\text{C}$.

This study showed that sulfur oxides and CO_2 evaporated during heating of the glass batches. Of course, evaporated water and ammonia were also released from the glass batches. It is essential to confirm this due to the limits placed on activities releasing pollutants into the environment. In addition, the glasses described are to be used as glass fertilizers. The HT-XRD results showed that magnesium silicate and phosphates were formed during heating of the glass batches.

Understanding these batch-to-glass conversion processes is fundamental to developing technology for obtaining glasses.

Acknowledgements This work was funded by the National Science Centre, Poland, project number 2018/31/D/ST8/03148.

Declarations

Conflict of interest The authors declare that they have no known competing financial interests or personal relationships that could have appeared to influence the work reported in this paper.

Open Access This article is licensed under a Creative Commons Attribution 4.0 International License, which permits use, sharing, adaptation, distribution and reproduction in any medium or format, as long as you give appropriate credit to the original author(s) and the source, provide a link to the Creative Commons licence, and indicate if changes were made. The images or other third party material in this article are included in the article's Creative Commons licence, unless indicated otherwise in a credit line to the material. If material is not included in the article's Creative Commons licence and your intended use is not permitted by statutory regulation or exceeds the permitted use, you will need to obtain permission directly from the copyright holder. To view a copy of this licence, visit <http://creativecommons.org/licenses/by/4.0/>.

References

1. ECOSOC "Problems of the human environment: report of the secretary-general," Forty-seventh Sess. (New York, 26 May 1969), 1969.
2. G M M SCALET Bianca Maria, R S SISSA Aivi Querol, and D S Luis, "JRC reference report. Best available techniques (BAT) reference document for the manufacture of glass," 2013. [Online]. Available: file:///C:/Users/Justyna/Downloads/Ifna25786enn.pdf.

3. Verheijen O S and Beerkens R G C. Thermal and chemical behavior of glass forming batches. vol PhD, no. 2003. 2003.
4. Collignon J, Rongen M, Beerkens R. Gas release during melting and fining of sulphur containing glasses. *Glas Technol Eur J Glas Sci Technol Part A*. 2010;51(3):123–9.
5. Beerkens RGC. Sulphate decomposition and sulphur chemistry in glass melting processes. *Glas Technol*. 2005;46(2):39–46.
6. Albayrak G, Sengel H. Review of sulphate chemistry and its impact on glass production. *Glas Technol Eur J Glas Sci Technol Part A*. 2016;6:289–96.
7. Sergeev D, Yazhenskikh E, Kobertz D, Müller M. Vaporization behavior of Na₂CO₃ and K₂CO₃. *Calphad Comput Coupling Phase Diagrams Thermochem*. 2019;65(February):42–9. <https://doi.org/10.1016/j.calphad.2019.02.004>.
8. Heide K. Thermogravimetric and mass spectrometric investigations of the decomposition and volatilization of raw materials by heating of a glass batch. *J Therm Anal*. 1989;35(2):305–18. <https://doi.org/10.1007/BF01904433>.
9. Vernerová M, Němec L, Kloužek J, Hujová M. Gas release phenomena in soda-lime-silica glass. *J Non Cryst Solids*. 2018;500:158–66. <https://doi.org/10.1016/j.jnoncrysol.2018.07.058>.
10. Cheng J, Deng Z, Du X. Influence of granulation on the pre-reaction behaviour of glass batches. *Glas Technol Eur J Glas Sci Technol Part A*. 2013;54(1):20–4.
11. Dolan MD, Misture ST. Analysis of glass batch reactions using in situ x-ray diffraction. Part I. Batch components and binary quartz mixtures. *Glas Technol*. 2004;45(3):140–7.
12. Deng W, Wright R, Boden-Hook C, Bingham PA. Melting behavior of waste glass cullet briquettes in soda-lime-silica container glass batch. *Int J Appl Glas Sci*. 2019;10(1):125–37. <https://doi.org/10.1111/ijag.12555>.
13. Xu K, Hrma P, Rice J, Riley BJ, Schweiger MJ, Crum JV. Melter feed reactions at T ≤ 700 °C for nuclear waste vitrification. *J Am Ceram Soc*. 2015;98(10):3105–11. <https://doi.org/10.1111/jace.13766>.
14. Rodriguez CP, Chun J, Schweiger MJ, Kruger AA, Hrma P. Application of evolved gas analysis to cold-cap reactions of melter feeds for nuclear waste vitrification. *Thermochim Acta*. 2014;592:86–92. <https://doi.org/10.1016/j.tca.2014.06.022>.
15. Vernerová M, Kloužek J, Němec L. Reaction of soda-lime-silica glass melt with water vapour at melting temperatures. *J Non Cryst Solids*. 2015;416:21–30. <https://doi.org/10.1016/j.jnoncrysol.2015.02.020>.
16. Beerkens R. “69th conference on glass problems,” vol. 53, no. 9, pp. 1689–1699, 2008.
17. Sułowska J, Madej D, Pokrzywka B, Szumera M, Kruk A. Structural and optical properties of pure and sulfur-doped silicate – phosphate glass. *Molecules*. 2021;26:1–28.
18. Kosińska-Pezda M, Zapała L, Maciołek U, Byczyński Ł, Woźnicka E, Zapała W. Thermal study temperature diffraction patterns and evolved gas analysis during pyrolysis and oxidative decomposition of novel ternary complexes of light lanthanides with mefenamic acid and 110-phenanthroline. *J Anal Appl Pyrolysis*. 2021. <https://doi.org/10.1016/j.jaap.2021.105293>.
19. Brahim K, Rouissi K, Soussi-Baatout A, Khattech I. Thermochemistry and kinetics of the aspect of diammonium hydrogen phosphate precipitation in phosphoric acid solution. *J Therm Anal Calorim*. 2021;143(4):3173–9. <https://doi.org/10.1007/s10973-020-09399-z>.
20. Mcadam AC, et al. “Journal of geophysical research : planets.” *Figure*. 2014;1:373–93. <https://doi.org/10.1002/2013JE004518>.
21. N. I. of S. and T. Standards, “NIST chemistry webbook,” NIST standard reference database number 69. <https://webbook.nist.gov/chemistry/>.
22. Wang Z, et al. Thermochemical behavior of three sulfates (CaSO₄, K₂SO₄ and Na₂SO₄) blended with cement raw materials (CaO-SiO₂-Al₂O₃-Fe₂O₃) at high temperature. *J Anal Appl Pyrolysis*. 2019;142:104617. <https://doi.org/10.1016/j.jaap.2019.05.006>.
23. Jin J, Zhou W, Sun Y, Han Y, Li Y. Reaction characteristics and existing form of phosphorus during coal-based reduction of oolitic iron ore. *Minerals*. 2021;11(3):247. <https://doi.org/10.3390/min11030247>.
24. Bourgel C, Véron E, Poirier J, Defoort FO, Seiler JM, Peregrina C. Behavior of phosphorus and other inorganics during the gasification of sewage sludge. *Energy Fuels*. 2011;25(12):5707–17. <https://doi.org/10.1021/ef201308v>.
25. Czakis-Sulikowska D, Radwańska-Dočekalska J, Czyłkowska A, Goluchowska J. TG-MS, TG, DTG and dta methods in study of thermal decomposition of some d-metal complexes with 4,4'-bpy and propionates. *J Therm Anal Calorim*. 2004;78(2):501–11. <https://doi.org/10.1023/B:JTAN.0000046114.02441.c3>.
26. Pardo A, Romero J, Ortiz E. Higherature behaviour of ammonium dihydrogen phosphate. *J Phys Conf Ser*. 2017;935:1. <https://doi.org/10.1088/1742-6596/935/1/012050>.
27. Risoluti R, Piazzese D, Napoli A, Materazzi S. Study of [2-(2'-pyridyl)imidazole] complexes to confirm two main characteristic thermoanalytical behaviors of transition metal complexes based on imidazole derivatives. *J Anal Appl Pyrolysis*. 2016;117:82–7. <https://doi.org/10.1016/j.jaap.2015.11.018>.
28. Matusiak J, Maciołek U, Kosińska-Pezda M, Sternik D, Orzel J, Grządka E. Textural and thermal properties of the novel fucoidan/nano-oxides hybrid materials with cosmetic, pharmaceutical and environmental potential. *Int J Mol Sci*. 2022. <https://doi.org/10.3390/ijms23020805>.
29. Lewis JMT, et al. Pyrolysis of oxalate acetate and perchlorate mixtures and the implications for organic salts on mars. *J Geophys Res Planets*. 2021;126:4. <https://doi.org/10.1029/2020JE006803>.
30. Santrock J, Studley SA, Hayes JM. Isotopic analyses based on the mass spectra of carbon dioxide. *Anal Chem*. 1985;57(7):1444–8. <https://doi.org/10.1021/ac00284a060>.
31. Emmerich WD, Kaisersberger E. Simultaneous TG-DTA mass-spectrometry to 1550°. *J Therm Anal*. 1979;17(1):197–212. <https://doi.org/10.1007/BF02156617>.
32. Kloužek J, Arkosiová M, Němec L. Redox equilibria of sulphur in glass melts. *Ceram - Silikaty*. 2006;50(3):134–9.
33. Tsujimura T, Tanaka C, Sakamoto O. Melting reactions in a granulated Na₂O-CaO-SiO₂ glass batch studied by x-ray diffraction and mass spectroscopy. *Glas Technol Eur J Glas Sci Technol Part A*. 2012;53(5):202–10.
34. R. L. Lehman, J. S. Gentry, and N. G. Glumac, “Thermal stability of potassium carbonate near its melting point [https://doi.org/10.1016/S0040-6031\(98\)00289-5](https://doi.org/10.1016/S0040-6031(98)00289-5) : *Thermochimica Acta | ScienceDirect.com*,” vol. 316, pp. 1–9, 1998, [Online]. Available: <http://www.sciencedirect.com/science/article/pii/S0040603198002895>.
35. Huang Y, et al. Release and transformation pathways of various K species during thermal conversion of agricultural straw. part I: devolatilization stage. *Energy Fuels*. 2018;32(9):9605–13. <https://doi.org/10.1021/acs.energyfuels.8b02191>.
36. Stern K and Weise E L. High temperature properties and decomposition of inorganic salts. Part 2. Carbonates. Washington, 1969.
37. C and G N Flick,. Redox conditions during the melting of batch. *Glas Sci Technol*. 1995;68:81–3.
38. Sułowska J, Jeleń P, Olejniczak Z, Szumera M. Sulfur speciation and network structural changes in silicate-phosphate glasses. *J Non Cryst Solids*. 2021. <https://doi.org/10.1016/j.jnoncrysol.2021.120645>.
39. Tesfaye F, Lindberg D, Moroz M, Hupa L. Investigation of the K-Mg-Ca sulfate system as part of monitoring problematic

- phase formations in renewable-energy power plants. *Energies*. 2020;13:20. <https://doi.org/10.3390/en13205366>.
40. Ueda N, et al. Conversion kinetics of container glass batch melting. *J Am Ceram Soc*. 2021;104(1):34–44. <https://doi.org/10.1111/jace.17406>.
 41. Zheng C, Wang Y, Liu Y, Yang Z, Qu R, Ye D, Liang C, Liu S, Gao X. Formation, transformation, measurement, and control of SO₃ in coal-fired power plants. *Fuel*. 2019;241:327–46. <https://doi.org/10.1016/j.fuel.2018.12.039>.
 42. Boström D, et al. Ash transformation chemistry during combustion of biomass. *Energy Fuels*. 2012;26(1):85–93. <https://doi.org/10.1021/ef201205b>.
 43. Grimm A, Skoglund N, Boström D, Öhman M. Bed agglomeration characteristics in fluidized quartz bed combustion of phosphorus-rich biomass fuels. *Energy Fuels*. 2011;25(3):937–47. <https://doi.org/10.1021/ef101451e>.
 44. Billen P, Van Caneghem J, Vandecasteele C. Predicting melt formation and agglomeration in fluidized bed combustors by equilibrium calculations. *Waste Biomass Valorization*. 2014;5(5):879–92. <https://doi.org/10.1007/s12649-013-9285-0>.
 45. Jung IH, Hudon P. Thermodynamic assessment of P 2O 5. *J Am Ceram Soc*. 2012;95(11):3665–72. <https://doi.org/10.1111/j.1551-2916.2012.05382.x>.

Publisher's Note Springer Nature remains neutral with regard to jurisdictional claims in published maps and institutional affiliations.